

# We are IntechOpen, the world's leading publisher of Open Access books Built by scientists, for scientists

5,800

Open access books available

142,000

International authors and editors

180M

Downloads

Our authors are among the

154

Countries delivered to

TOP 1%

most cited scientists

12.2%

Contributors from top 500 universities



WEB OF SCIENCE™

Selection of our books indexed in the Book Citation Index  
in Web of Science™ Core Collection (BKCI)

Interested in publishing with us?  
Contact [book.department@intechopen.com](mailto:book.department@intechopen.com)

Numbers displayed above are based on latest data collected.  
For more information visit [www.intechopen.com](http://www.intechopen.com)



Chapter

# Parameters Affecting Pre-Treatment Dosimetry Verification

*E. Ishmael Parsai and Elahheh Salari*

## Abstract

To assure the accuracy and safety of radiation delivery, it is highly recommended to perform pretreatment verification for complex treatment methods such as intensity-modulated radiation therapy (IMRT) or volumetric-modulated arc therapy (VMAT) to detect any potential errors in the treatment planning process and machine deliverability. It is expected that a qualified medical physicist is aware of the underlying scientific principles of imaging and therapeutic processes to perform or supervise technical aspects of pretreatment procedures to ensure safe and effective delivery of the treatment. For this purpose, several guidelines have been published to help direct medical physicists to evaluate the accuracy of treatment planning system (TPS) in the calculation of radiation dose, and dosimetry equipment to avoid possible errors. This will require a clear understanding of abilities as well as the limitations of each TPS, the dosimetry equipment at hand, and the gamma index to perform a comprehensive pre-treatment verification.

**Keywords:** pre-treatment verification, gamma index, treatment planning algorithms, beam modeling, detector resolution, planned dose grid, modulation index

## 1. Introduction

As a treatment modality driven by technology, radiation therapy (RT) has made significant advances in recent years. These advances have mostly been in areas of treatment delivery, imaging, and image fusion which has required sophisticated algorithms for calculation of dose in patients and complex machines to deliver the dose. There is always some level of discrepancies between the calculated dose and delivered dose which can arise from different sources such as: the dose calculation algorithm, beam modeling in TPS, physics data entry, beam delivery, detector resolution, and planned grid size. The purpose of this chapter is to present a review of algorithms for photon dose calculation, beam modeling in different TPSs, detector resolution and planned grid size (GS) and analyze the effect of each of them on gamma passing rate (GPR) in pre-treatment quality assurance (QA).

## 2. Treatment planning system (TPS) algorithms

For understanding TPS algorithms, it is required to know [1]:

1. The production of Megavoltage X-rays
2. The interaction and scattering of photons by the Compton effect
3. The effects of transport of charged particles near boundaries and tissue heterogeneities

By far, medical linear accelerators (linac) are the main devices used in the treatment of cancer patients producing X-rays and electrons in the clinical energy range. In the head of a linac, high energy electrons are accelerated to the near speed of light and are directed to strike a high Z target typically made of Tungsten which has also a high melting point to produce photon. The bremsstrahlung photons produced by a linac have an energy distribution from 0 to maximum energy of the electrons in the beam impinging upon the target. These photons pass through the primary collimator and other parts of the linac head such as jaws, Multi Leaf Collimator (MLC) system, etc. before reaching the patient. All these photons (primary and scattered) will contribute to photon fluence. For example, for a typical Varian linac with a flattening filter, 80–90% of primary photons are directly from the target, 3–5% from the primary collimator, 8–12% originated from the flattening filter [1, 2]. However, in modern linacs which are equipped with flattening filter free (FFF) technology, scatter photon produced in the treatment head has significantly decreased [3, 4]. Therefore, the contribution of primary and scatter photon in photon fluence for FFF is different from the flattened beam [5]. For example for a  $40 \times 40 \text{ cm}^2$  field size and a 6 MV FFF beam, the calculated contribution was 84.6% for the primary source, 11.3% for the first scattered source, and 4.1% for the second scattered source [5].

In general, ionizing radiation such as photon, electron, and heavy charged particles interact with matter which depends on the energy of ionizing radiation, type of ionizing radiation, the atomic number, and density of the medium through which they travel. Photons are indirect ionizing radiation and energy deposition of the photon to the material is dominated by three interactions: Photoelectric, Compton scatter, and pair production. In the energy range from 100 Kev to 10 MeV, which is a mostly therapeutic range, the Compton process is dominant for energy absorption in soft tissues. The energy deposition of photons involves two stages: First, partial transfer of their kinetic energy to charged particles (electron, positron) when they interact with material, and second, energy deposition from these charged particles to material through excitation or ionization. The range of charged particles in the therapeutic energy range can be several centimeters so they can travel and pass-through various layers with different densities and atomic numbers in a human body. When charged particle equilibrium (CPE) is achieved, then there is a linear relationship between TERMA<sup>1</sup> (Total energy released per unit mass) and dose, and the two steps can be included in a single calculation. However, this condition does not occur near the edge of the field or in inhomogeneity regions like at tissue interfaces, therefore, this

---

<sup>1</sup> the production of mass attenuation coefficient and primary energy fluence of photon

simplification cannot be valid, and the two steps of energy deposition of the photon to medium must be more clearly distinguished [6].

The human body consists of a variety of tissues and cavities that are radiologically different from water, such as lungs, oral cavities, teeth, nasal passages, sinuses, and bones. A treatment planning system uses the electron density derived from CT images of patients to calculate dose in the patient body. Therefore, the dose distribution inside the patient body is affected by these heterogeneities. In this area, the ability of treatment planning systems to calculate dose at the interferences such as lung vs. tissue, bone vs. air cavity, etc. is crucial. Also, using CT images with 3D TPS allows us to design a plan with complex beam arrangements which require more advanced dose computation algorithms. In this section, we will present a summary review of the past and current dose calculation algorithms used in the TPS for radiotherapy.

According to the American Association of Physicists in Medicine (AAPM) Task Group 65 (TG-65, Report No.85) [6], there are four types of inhomogeneity correction algorithms:

Category.1: Linear attenuation, Ratio of tissue air ratio (RTAR), Power law (Batho).

Category.2: Equivalent TAR, Differential scatter air ratio (dSAR), Delta volume, Differential TAR, and 3D Beam subtraction method.

Category.3: Convolution (pencil beam) and Fast Fourier transformation (FFT) techniques.

Category.4: Superposition/Convolution, Monte Carlo.

## 2.1 Category.1

### 2.1.1 Linear attenuation

This is the simplest technique for computation of inhomogeneity correction factor (ICF), which does not include any information regarding electron density and the geometric treatment beam parameters such as field size [6].

$$ICF = (\% \text{ per } cm) \times \text{inhomogeneity thickness (cm)} \quad (1)$$

### 2.1.2 Ratio of tissue air ratio (RTAR)

Only heterogeneity correction applied on the beam path from source to the calculation point.

$$ICF(d, r) = \frac{TAR(d', r)}{TAR(d, r)} \quad (2)$$

where  $d$  and  $d'$  are physical depth and water equivalent depth to the calculation point and  $r$  is the field size at depth  $d$ . The main weakness of this method is overcorrection when the density of the medium is less than the density of the water and under correction when the density is greater than the density of water due to compromised modeling of lateral component of the scattered photon [7].

### 2.1.3 Power law (Batho)

This is an empirical correction factor method for points lying within water and distal to an inhomogeneity by raising tissue-air ratios to a power that depends on

density. This was first proposed by Batho in 1964 [8] and then modified by Sontag and Cunningham in 1977 [9].

$$ICF = \frac{TAR(d_1, r)^{\rho_1 - \rho_2}}{TAR(d_2, r)^{1 - \rho_2}} \quad (3)$$

where  $d_1$  is depth to first slab boundary and  $d_2$  is depth to second slab boundary from the point of calculation at depth  $d$ .  $r$  is field size at depth  $d$  and  $\rho_1$  and  $\rho_2$  are densities of the medium in which the calculation point is located and relative electron density of the overlying material respectively.

The power law method underestimates the dose when density is less than one and overestimates when density is greater than one [6]. Several studies showed improvement if Tissue Maximum Ratio (TMR) is used instead of TAR [10, 11].

## 2.2 Category.2

### 2.2.1 Equivalent TAR (ETAR)

It can be considered as the first practical dose calculation method using the full CT data set for computerized treatment planning and was used in early treatment planning systems [6].

$$ICF(d, r) = \frac{TAR(d', \tilde{r})}{TAR(d, r)} \quad (4)$$

where  $d'$  and  $\tilde{r}$  represent the “scaled” or “effective” values of depth at interesting point ( $d$ ) and field radius ( $r$ ) respectively for the energy of the radiation being used. This method required excessive computer memory and calculation times; therefore, some adjustments such as the coalescing of adjacent CT slices were applied to reduce 3D calculations to appropriate 2D calculations to make it more practical for use in clinics in the 1980s.

### 2.2.2 Differential scatter air ratio (dSAR)

This was a 3D dose calculation in a heterogeneous media that used scatter-air ratios (SAR) to calculate the dose to a point in an inhomogeneous medium. For this purpose, a SAR table was used to determine the scatter contribution that arises from voxels within the irradiation volume [12].

### 2.2.3 Delta volume (DVOL)

The primary dose, an analytical first-scatter dose component, and an approximate residual multiple-scatter component were summed to calculate dose at a point in a heterogeneous medium. This method has been examined and justified for Co-60 and succeeds in correctly calculating the dose to (a) water with a small void and, (b) homogeneous non-water medium.

dSAR and DVOL have never been implemented in clinics due to the long CPU time required to run them with no significant improvement in dose calculation accuracy compared to previously used algorithms [7].

## 2.2.4 Differential TAR

Kappas and Rosenwald [13] showed that applying  $K(\theta, \mu)$  on dSAR method results in more accurate results.

$$K(\theta, \mu) = e^{(\mu_0 \cos \theta - \mu_1(\theta))(\bar{b} - b)} \quad (5)$$

where  $\mu_0$  and  $\mu_1$  are the linear attenuation coefficients in the water of the primary and of the first-order scattered photons arriving at a point after a deflection.  $\bar{b}$  is the path length en route to point (in the waterlike medium) and  $b$  is the corresponding effective path length (in the heterogeneous medium). For very large fields and depths and when the thickness of the overlying tissue is greater than 5 cm, the difference between measurement and calculation is more than 2% and less than 6% [6].

In general, categories 1 and 2 are not applicable when photon energy is greater than 6MV where scatter contribution is less important, and the effects of secondary electrons (delta rays) set in motion can result in very high local dose changes [6].

## 2.3 Category.3

### 2.3.1 Convolution techniques

This technique is a model-based algorithm which unlike correction-based algorithms uses heterogeneity effects directly to compute the dose in tissue. Kernels are used for modeling the dose distribution in media. The kernels represent the energy spread and dose deposition of secondary particles from an interaction at a given point or line which is not usually accessible through measurements but is very simple to calculate by use of Monte Carlo particle transport codes [12]. Absorbed dose is calculated based on the following equation

$$\text{Absorbed Dose} = \text{energy fluence distribution} \otimes K \quad (6)$$

This means that the energy fluence distribution is *convolved*<sup>2</sup> with the scatter spread kernel (K) to obtain the dose.

*Energy deposition Kernel (EDK)* is the energy distribution revealed to volume elements (per unit volume) in an irradiated medium, commonly water. There are three different categories for EDKs based on the geometry of the elemental beam that delivers the incident energy: A point kernel, pencil kernel, and planar kernel [7].

**Point Kernel:** This kernel describes the pattern of energy deposition in an infinite media around a primary photon interaction site.

**Pencil Kernel:** This kernel describes the energy deposition in a semi-infinite medium from a point monodirectional beam.

**Planar Kernel:** A planar kernel describes the energy spread from primary interactions located in a plane of an infinite broad beam.

In 1986, Mohan et al. [14] introduced a *differential Pencil beam algorithm* which is a good example of this category. This is the simplest and fastest algorithm for dose calculation because it only considers inhomogeneity corrections in longitudinal

<sup>2</sup> Convolution,  $\otimes$ , is a mathematical operation used to combine functions.

direction in the central beam axis and ignores lateral scatter. Therefore, it does not accurately model the distribution of secondary electrons in heterogeneous media. This limitation causes inaccurate dose calculation in heterogeneous treatment sites such as the lung, bone, or interfaces [15, 16].

### 2.3.2 Fast Fourier transform (FFT) convolution

This technique reduces computation time greatly because of the invariant kernel assumption for the convolution calculation. Because of this assumption, different kernels at different regions based on the density cannot be used in FFT. Several studies were conducted to circumvent invariant kernel assumptions [17–19]. In 1996, Wong et al. [20] proposed a solution to address problems related to lateral disequilibrium and penumbra in low-density regions because a water kernel was used for entire regions even in low-density regions. The lateral disequilibrium problem was solved by *lateral* scaling of the field size at each depth according to local effective densities to adjust the dose along the central axis in heterogeneities. This technique is based on the ETAR method, by convolving the density at the intersection site with the primary kernel for water. The resultant dose distribution is then inverse scaled according to the effective density to correct the penumbra problem which accounts for the electron transport near the field edge inside a low-density medium with or without lateral disequilibrium.

## 2.4 Category.4

### 2.4.1 Convolution-superposition algorithms

The convolution-superposition algorithm is also a model-based algorithm and has two essential parts: 1) TERMA and 2) dose spread kernel. TERMA was first introduced by Ahnesjo et al. in 1987 [21] which is analogous to the Kerma, (the kinetic energy released in medium) and has the same unit as dose. The formula for the TERMA element (T) of the convolution method is given by the following equation

$$T(\vec{r}') = \frac{\mu}{\rho}(\vec{r}', E) \cdot \Psi(\vec{r}') \quad (7)$$

where  $\mu/\rho$  is the mass attenuation coefficient and  $\Psi$  is the primary energy fluence. Then the convolution-superposition is the integration of the TERMA distribution times EDK over the entire volume. EDK is spatially variant and is deformed based on the local density environment to consider interface effects in regions of different densities. Also, to get a more accurate model of the scattering conditions, the kernels must be adjusted according to their direction and orientation at the site of interaction [22].

This method is widely used in TPS because computers are fast enough to do 3D dose calculations by using electron density data derived from CT images in a reasonable amount of time. According to AAPM report 85 (TG-65), the dose calculation accuracy of TPS algorithms should be within 2%. This goal serves as a useful benchmark to evaluate the capabilities of treatment planning algorithms to calculate the dose.

### 2.4.2 Anisotropic analytical algorithm

Anisotropic Analytical Algorithm (AAA) (Varian Medical System, Inc) is a kernel-based convolution-superposition method. This algorithm was first designed by Ulmer

and Kaissl (2005) [23] in cylindrical coordinate and then improved by Tillikainen in 2008 [24]. The AAA dose calculation model has two main components, the configuration algorithm, and the actual dose calculation algorithm. Its configuration is based on the Monte Carlo simulations to determine basic physical parameters and match them with measured clinical beam data. The dose calculation algorithm utilizes separate models for primary photons, scattered extra-focal photons, and contamination electrons. The lateral distribution is adjusted according to the radiological distance to the calculation point for tissue heterogeneities corrections [16, 25]. For the most part, AAA is a pencil beam convolution-superposition algorithm where the pencil beam is compiled from Monte Carlo calculations and adjusted to fit measurements. In this case, two components need to be considered that contribute to final distributions; 1) longitudinal contribution of the pencil beam which is scaled according to Equivalent Length Path (EPL), and 2) contribution from the lateral extension of the pencil beam which is scaled with the density relative to water in directions normal to the pencil beam [26]. In this way, the changes in lateral transport of energy are modeled when the density varies in the irradiated object. Therefore, unlike the pencil beam algorithms, it can consider inhomogeneity correction on both longitudinal and lateral directions. However, many studies indicate the inability of AAA to accurately calculate doses at interfaces and for high atomic number materials such as bone and have shown that the deviation between AAA and measurements exceeds the goal of TG-65 [27–30].

The advantage of the AAA is its relatively short calculation time and its accuracy is better than the pencil beam convolution (PBC) model [30–32].

#### 2.4.3 Collapsed cone convolution

In 1989 Ahnesjo [33] proposed collapsed cone convolution (CCC) method. The CCC algorithm uses the analytical kernel in polar coordinates represented by a set of cones. In this way, it is assumed that all energy is released into coaxial cones of equal solid angle and, from volume elements on the cone axis is approximated to be rectilinearly transported, attenuated, and deposited in volume elements on that axis [7]. The polyenergetic kernels can be described by

$$h(r, \theta) = \frac{A_{\theta}e^{-\alpha_{\theta}r} + B_{\theta}e^{-b_{\theta}r}}{r^2} \quad (8)$$

where  $A_{\theta}$ ,  $\alpha_{\theta}$ ,  $B_{\theta}$ , and  $b_{\theta}$  are fitting parameters depending on the scattering angle  $\theta$  and  $r$  is radial distance. The first term mainly describes the primary dose and the second term is the scatter dose fraction.

The advantage of the CCC algorithm over standard convolution algorithms is that it can reduce the computation resources. The computation time for the CCC method in heterogenous media is proportional to  $MN^3$  where  $M$  is the number of cones and  $N$  is the number of voxels along one side of the calculation volume [16]. Different TPSs use the CCC algorithm such as Pinnacle (Philips Inc., Amsterdam, Netherlands), Oncentra MasterPlan (Nucletron, Inc., Columbia, MD, USA), CMS XiO (Elekta AB, Stockholm, Sweden), RayStation (RaySearch Laboratories AB, Stockholm, Sweden), etc.

#### 2.4.4 Monte Carlo

Monte Carlo (MC) is a principle-based algorithm that almost includes all known physical features for photon interactions inside the patient body. Many MC codes



have been developed such as BEAMnrc, GEANT4, MNCP, PENELOPE, and XVMC. All of them have two main steps, first, modeling the linac head with all precise details of the target, component dimensions, geometry, locations, and material composition. The second step uses CT data to get morphological and chemical information in terms of mass density, electron density, and atomic composition, which are all required for accurate dose calculation in the tissue.

The MC has the capability of simulating all interactions, therefore it is expected to be accurate. However, its accuracy depends on correct and detailed geometry information of the linac head and the number of particle histories. This statistical uncertainty is proportional to the inverse square root of the generated event numbers [34, 35]. MC dose calculation is slow and time-consuming, so they are not yet applicable in clinics because the dose may recompute repeatedly during planning to get an optimized plan. A few vendors offer Monte Carlo methods in TPS as calculation options for the final dose calculation once the dose optimization is completed.

#### *2.4.5 Acuros XB*

Monte-Carlo (MC) dose calculation algorithm is widely considered as the golden dose calculation technique in radiation therapy; however, the calculation time of this method is still long especially where a greater number of particle histories should be used to reduce statistical noise and/or a high spatial resolution is required. An alternative method to MC is the linear Boltzmann transport equation (LBTE) method which solves LBTE refers to grid-based Boltzmann solver (GBBS). GBBS solves the LBTE through discretizing photon and electron fluences in space, energy, and angle to allow a deterministic solution of the transport of radiation through matter. Its calculation accuracy is comparable to MC, and both are convergent methods because the MC algorithm simulates an infinite number of particles, GBBS discretizes the LBTE variables into infinitely small grids, then the two methods should converge to the real solution. However, MC and GBBS have different sources of error, there is statistical noise due to simulating a finite number of particles in Monte Carlo, while most errors in GBBS methods are systematic and their main source is discretization of the solution variables in space, angle, and energy [36, 37]. An algorithm using this technique is based on Attila (Los Alamos National Laboratory, Los Alamos, NM, and Transpire Inc., Gig Harbor, WA). Attila employs linear discontinuous finite-element spatial differencing on a computational mesh consisting of arbitrary tetrahedral elements. The primary photon fluence is analytically transported through ray tracing, and the discrete ordinates method is used for angular differencing of the scattered fluence. Based on Attila, a dose calculation algorithm for external photon beams has been developed on the same methods and implemented in the Varian Eclipse external beam treatment planning system (Varian Medical Systems, Palo Alto, CA, USA) [38]. This new deterministic radiation transport algorithm is Acuros XB (AXB), and it has been well shown by several studies that the accuracy of dose calculation of AXB is more accurate than AAA and is very similar to MC dose calculations [36–38].

### **3. Beam Modeling of commercial treatment planning systems**

In radiotherapy, the ability of TPS to do accurate dose calculation is important. This capability depends on the algorithm of TPS as discussed before and beam

modeling. For beam modeling, several dosimetric parameters (e.g., PDDs, profiles, output factors) and non-dosimetric parameters such as MLC design, flattening filter, wedges etc. must be defined precisely. Then the dose calculation algorithm applies the beam model to the patient body or phantom to calculate the dose. The challenge of the beam model is becoming more and more crucial due to advanced treatment techniques such as IMRT and VMAT. In these treatment techniques, each beam consists of multiple segments or control points that are shaped with MLC. Using multiple control points provides this opportunity to deliver conformal dose to the target, however, delivering dose through small segments arises a challenge to accurately calculate the dose due to the complexity of MLC modeling in TPS. Many studies indicate the importance of accurate MLC modeling in TPS for IMRT. In 1998, LoSasso et al. [39] showed an MLC error gap of 1 mm may result 10% error in dose calculation in the sliding window IMRT technique. Cadman et al. [40] reported 12% discrepancy between calculation and measurement due to MLC leaf gap error in step-and-shoot IMRT. Because different commercial TPS have their own features for beam modeling, many guidelines have been published regarding TPS commissioning for IMRT [41, 42]. For example, TG-119 [43] based on the IMRT QA results of five institutions for a set of test cases provides a reference baseline for the accuracy of IMRT commissioning.

In Eclipse, leaf transmission factors and dosimetric leaf gaps (DLGs) are required to model the MLC. The DLG is a beam configuration parameter used to model the effects of rounded MLC leaf ends. Many research papers indicate the effects of DLG on the accuracy of dose calculation in Eclipse TPS [44–47].

In RayStation, modeling of MLC is different from other commercial TPS. The MLC model requires four parameters: leaf-tip offset, leaf-tip width, average transmission factor, and tongue and groove. The leaf-tip width is used for the MLC leaf-end transmission modeling instead of using dosimetric leaf gap (DLG) or rounded leaf-tip radius, and the MLC leaf radiation transmission is modeled using average transmission factor instead of intra-leaf and inter-leaf transmission [48, 49]. According to Chen et al. tongue-and-groove has a minimal effect on IMRT dose calculation, but transmission plays a significant role in this commercial TPS [49].

## **4. Measurement methods for pre-treatment verification**

The process of patient-specific QA usually involves applying an optimized plan using the same beam parameters as those of the patient plan and delivered in the phantom. This process can be done in a number of different ways but according to TG-218 [50], there are three common methods for performing pre-treatment QA. 1) True Composite (TC), 2) Perpendicular field-by-field (PFF), and 3) Perpendicular composite (PC).

### **4.1 True composite**

In this method, phantom or measurement device is placed on the treatment couch and treatment plan is delivered using actual parameters such as MUs, couch, gantry, collimator angles, MLCs, and jaws positions. The phantom or measurement device has been used to integrate dose from all beams of a plan which result in a single dose image for comparison, therefore, this method is a comparison of planned dose vs. measured dose.

## 4.2 Perpendicular field-by-field

The gantry is fixed at zero degree and the collimator is fixed at the nominal angle in the PFF technique. Therefore, beams are always perpendicular to the phantom surface and are comparing the dose of each beam with each measured beam dose.

## 4.3 Perpendicular composite

This method is similar to the PFF method, but this is not a comparison of field-by-field. This is the integration dose of all perpendicular field which result in one dose image for analysis.

## 5. Gamma index

For the purpose of dose comparisons between calculated and measured dose gamma index have been used. Low et al. [51] developed a gamma index ( $\gamma$ ) for the quantitative evaluation of dose distributions. This index checks dose difference and distance-to-agreement (DTA) simultaneously in a space that also includes dose, and provides quantitative value which indicates disagreement in the regions that fail the acceptance criteria. A  $\gamma$  comparison is performed between two dose maps: one distribution is the 'reference dose distribution' and the other is the 'evaluated dose distribution'. The *reference dose distribution* is referred to as true distribution so it is usually measured data using devices such as ion chamber, film, diode array detector etc., and the *evaluated dose distribution* is analyzed for its agreement with the reference and can be the predicted TPS dose distribution. To avoid any confusion, low replaced reference and evaluated terms by measured and calculated respectively. The gamma index calculation is based on Eq. (9):

$$\Gamma(r_R, r_E) = \sqrt{\frac{\Delta r^2(r_R, r_E)}{\delta r^2} + \frac{\Delta D^2(r_R, r_E)}{\delta D^2}} \quad (9)$$

where  $r_R$  and  $r_E$  are reference points and evaluated point respectively,  $\delta r$  is distance difference criterion and  $\delta D$  is the dose difference criterion.  $\Delta D$  is dose difference which is calculated using Eq. (10):

$$\Delta D(r_R, r_E) = D_E(r_E) - D_R(r_R) \quad (10)$$

$D_E$  and  $D_R$  are the doses at a point in evaluated dose distribution and reference dose distribution respectively.

The  $\gamma$  is the minimum value calculated overall evaluated points:

$$\gamma(r_R) = \min \{ \Gamma(r_R, r_E) \} \forall \{ r_E \} \quad (11)$$

Regions where  $\gamma$  is less than or equal to 1 corresponds to locations where the calculation meets the acceptance criteria. According to TG-218, criteria for tolerance limit is 2 mm/3% with 95% passing rate [50].

There are two types of gamma calculation which depends on how the percent dose difference (%Diff) is normalized: 1) local normalization method which %Diff is

normalized to the doses at each evaluated point, 2) global normalization method which %Diff is normalized usually to the maximum dose within the reference dose distribution. Each method has its own advantages and disadvantages. For example, local gamma will exaggerate %Diff and highlighted failures in low dose regions because in low dose regions the percent dose difference between calculated and measured may exhibit a very large value which results in more failing points. However, in the global method, the dose discrepancies in the low-dose regions could be underestimated which results in a higher passing rate than the local method [52, 53].

### 5.1 Effect of planned grid size on gamma passing rate

Low et al. [51] presented a powerful tool for dose distribution comparisons in a continuous environment; however, clinical comparisons are usually made between two dose distributions which are sampled at different spatial resolutions. The importance of spatial resolution was first analyzed by Depuydt *et al* in 2001 [54]. They indicated that the pixel size of the compared image needs to be small with respect to acceptance criteria and showed that large grid spacing in the discrete dose distribution, especially in high dose gradient regions causes overestimation of gamma values. Several investigators introduced different solutions to resolve this issue [54–56]. For example, Low and Dempsey [57] showed that by decreasing grid size to  $1 \times 1 \text{ mm}^2$ , the error in  $\gamma$  reduced to less than 0.2 even in high dose gradient areas. Furthermore, Schreiner et al. [58] reported changing the resolution of the evaluated distribution (from 2.5 mm to 0.24 mm) increase the pass rate from 80.9% to 91.3%. These results are attributed to the behavior of gamma search. When the pixel size of the evaluated distribution is large compared to the reference distribution, many reference pixels would be far away from the nearest evaluated pixel which results in more failing points. Thus, the  $\gamma$  value for many reference pixels reflects significant spatial misalignment purely as an artifact of the coarse evaluated resolution. When the resolution of the evaluated distribution is increased to match that of the reference distribution, this spatial artifact is eliminated because each reference point has a directly corresponding pixel in the evaluated distribution. Increasing the evaluated resolution also provides each reference point with a greater range of dose values for comparison. Based on TG-218 [50], there is a rule of thumb that the resolution of the evaluated (calculated) should be no greater than 1/3 of the DTA and the straightforward solution for reducing artifact in gamma calculation is interpolation when planned grid size is greater than 1 mm (for DTA = 3 mm).

## 6. Dosimetry equipment for pre-treatment verification

Modern radiotherapy techniques like IMRT and VMAT are highly complex modalities due to MLCs motions, gantry rotation, dose rate variation during beam delivery. The advantages of using these techniques are delivery of conformal radiation dose to the target while sparing the surrounding normal tissues and organs-at-risk (OAR) are significantly higher compared to conventional 3D techniques. However, due to the high degree of complexity of these techniques, it is strongly recommended to do pre-treatment verification before dose delivery. For this reason, different types of 2D or 3D detectors such as diode arrays, ionization chambers, film (e.g., Gafchromic film EBT3), electronic portal imaging device (EPID), etc. have been used to ensure that the prescribed treatment dose is delivered within the clinically

acceptable error tolerances. Regardless of the type of detector, all of this equipment has spatial limitations because of the discrete placement and physical separation of each detector which may affect GPR results [59, 60].

### 6.1 Effect of detector resolution on gamma passing rate

As it was mentioned before, phantoms or dosimeter devices used for performing patient-specific QA present spatial resolution limitations which may affect GPR results. Several research has been conducted to show the discrepancy of GPR within different phantoms with different spatial resolutions. Bruschi et al. [59] studied the effect of detector resolution on GPR. Three detectors (PTW OCTAVIUS 4D 729, 1500, and 100 SRS) used in five configurations with different resolutions were utilized in their study. This study indicates the detector resolution can significantly affect the SBRT pre-treatment verification results and a detector with high spatial resolution would be able to detect any kind of error such as those caused by MLC position, collimator, and gantry rotations, etc. In 2017 Woon et al. [61] worked on a similar subject and used three detectors with different resolutions (MapCHECK2, ArcCHECK, and EPID). They demonstrated that MLC errors of greater than 0.5 mm were not distinguishable in measured doses by the MapCheck2/ArcCHECK due to the inferior resolution caused by the large diode spacing relative to the resolution of the EPID. Bailey et al. [53] reported that detector arrays with low-spatial resolution may potentially affect the gamma index analysis by under sampling data. On the other hand, Steers et al. [62] indicated that different detectors show different error sensitivity which depends on the induced type of error and the GPR does not highly depend on detector spatial sampling. Moreover, they showed that increasing spatial sampling not only increase the GPR but also reduces error sensitivity in many cases. This is observed if the increase in the number of sampling results in a higher number of low dose points in the comparison than high dose points, an effect which is increasingly important for globally normalized gamma comparisons [62]. Salari et al. [63] also compared standard density vs. high density measurements of ArcCHECK phantom in Intensity Modulation Radiosurgery (IMRS) cases and compared the GPR values. As shown in **Figure 1**, the results of standard density mode had better GPR for each energy and planned dose grid which is also in good agreement with Steer et al. result. Note that 1 mm and 2 mm represent GS; 6 FFF and 10 FFF for 6 MV FFF and 10 MV FFF beam energies, respectively.

Hussein et al. [64] also conducted research on five commercial QA devices and analyzed the effect of detector resolution on  $\gamma$ . They concluded that different combinations of QA devices and software exhibit varying level of agreement for the same passing rate.

## 7. Modulation indices

Modern treatment techniques, such as IMRT and VMAT, have enabled the escalation of target dose with fewer side effects to the surrounding OARs by modulation of the treatment plans to achieve the desired dose distribution. In IMRT, MLCs are moving during treatment, thereby delivering a radiation field with a non-uniform intensity while in VMAT technique, in addition to MLC motions, gantry speed and dose rate are also variable when the radiation beam is continuously on. For patients' protection and safety, pretreatment dosimetric verification is done to provide

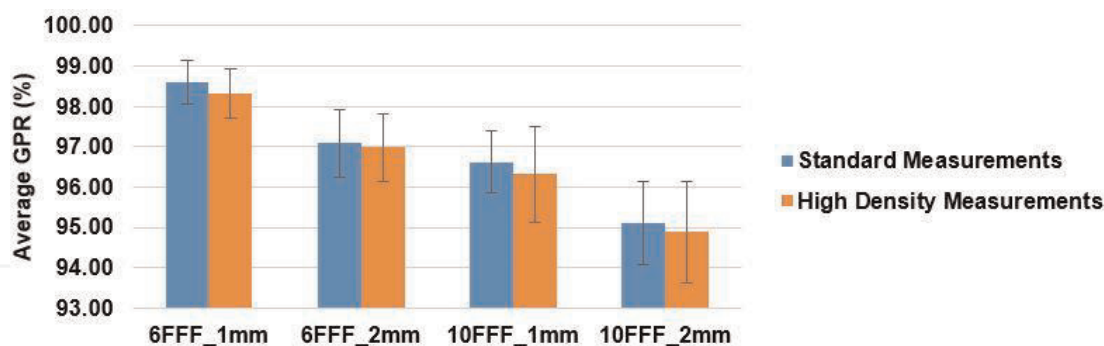


**Figure 1.** Comparisons of standard density vs. high-density modes between different planned grid sizes and energy. (reprinted from Salari, et al., “evaluation of parameters affecting gamma passing rate in patient-specific QA’s for multiple brain lesions IMRS treatments using Ray-Station treatment planning system. In print: *J Appl Clin med Phys.* 2021).

sufficient data on the safety and reliability of treatment plans and delivery, even though performing pretreatment dosimetric verification is considered an additional workload. Therefore, a retrospective analysis of which parameter (leaf travel, beam aperture and shapes, control point angular separation, dose rate, and gantry variations) can affect the ability of the TPS to calculate a dose may provide important information on the limits of TPSs for IMRT/VMAT plans. The difference between calculated and measured dose distribution may be affected by the accuracy of the TPS calculation and the delivery accuracy. Discriminating between the two causes of errors is not an easy task. Furthermore, the delivery accuracy of IMRT/VMAT plans can be predicted by the score of plan modulation complexity [65]. For this purpose, many authors introduced or evaluated different Modulation Indices (MI)/parameters to find a correlation between plan complexity and GPR.

Nicolini et al. [66] studied the effect of gantry speed (deg/s) and dose rate (MU/min) on the quality of VMAT plans and showed using a higher dose rate improves plan quality and reduces delivery time. They also used dynamic log files generated by linac controllers to evaluate the delivery accuracy of plans and found out accuracy slightly improved in delivery when using a low dose rate. Wu et al. [67] analyzed the results of dose verification of 924 patients including the relationship between gamma pass rates and the location of lesions, the total number of monitor units, and the maximum area of the collective dose. They observed a correlation between the treatment site and GPR plus a strong negative correlation between total MUs and GPR that indicates increasing MU results in lower GPR. Moreover, a weak negative correlation between the largest area of the acquisition dose and GPR was reported [67]. McNiven et al. [68] proposed *Modulation Complexity Score (MCS)* for step-and-shoot IMRT. This score is contribution of variability in the shape of segments and variations in their area. The range of MCS is from 0 to 1. The lower value of the MCS means higher complexity. This metric provides more information about the plan quality than simple metrics such as total MUs and number of segments, but no correlation was observed between GPR and MCS which is in a good agreement with other research [69, 70]. This index was later adapted by Masi et al. [65] for VMAT plans by substituting control points for segments and called it (MCSv). Also, Masi et al. introduced *Leaf Travel (LT)* as the average distance that MLC is traveling over one arc in VMAT and LTMCS index which takes into account both LT and MCSv and has a range between 0 and 1. Zero shows a higher degree of modulation and leaf motion. They reported a moderate correlation between LT, MCSv, LTMCS, and GPR

and a weak correlation between MU and GPR. Hernandez et al. [71] modified LT for multiple arcs or partial arc by dividing LT over arc length (LT/AL). Another index is *Edge Metric (EM)* which was defined by Young et al. [72] and it calculates the complexity as the ratio of MLC side length edge to aperture area. The larger EM index indicates the difference between the positions of adjacent leaves are larger which is closely related to the tongue-and-groove effect. Du et al. in 2014 [73] introduced several MIs to evaluate plan complexity such as *plan averaged beam area (PA)*, *plan averaged beam irregularity (PI)*, *plan averaged beam modulation (PM)*, and *plan normalized MU (PMU)*. PA is the average area of beam apertures; PI indicates the non-circularity of the shape of aperture and PM describes to what extent a beam is modulated with multiple smaller apertures. PMU is to compare the total MU among all plans with different prescription dose levels. According to a number of studies [70, 71, 73] MCS, EM, and PI provide similar information. In 2014, Park et al. [74] defined  $MI_s$ ,  $MI_a$ , and  $MI_{total}$  which  $MI_{total}$  unlike previous metrics include both gantry speed and dose rate variations besides MLC motions to quantify the total delivery complexity for VMAT plans.  $MI_s$  which evaluate MLC speed was originally introduced by Webb [75] to evaluate the modulation degree of IMRT and were modified by Park et al. for VMAT treatment plans and  $MI_a$  evaluates both speed and acceleration of MLCs. They also studied the MCSv and LTMCS and did not see correlations as high as those found in a previous study (Masi et al) to the pre-treatment VMAT QA results.

In summary, various studies were conducted in this area and revealed different results regarding the correlation between plan complexity indices and QA metrics [65–79]. We believe, these differences may depend on the linac model and its commissioning plus TPS limitations such as beam model, dose engine, and algorithm [71, 80, 81].

## 8. Conclusions

As described in this chapter, there are a number of sources which may contribute and arise different levels of discrepancy between the computed dose by TPS and measurements. Much effort has been devoted to improve the accuracy of dose calculation algorithms, computing technology and measurements, and through all these developments the accuracy of dose calculation and measurements seems close to our clinical goals. Although, the accuracy of dose calculation in homogenous medium (e.g., water) does not much rely on the algorithm, in heterogeneous media such as lungs or bone, the accuracy of calculation depends strongly on the kernels of calculation algorithms and how well they can simulate the actual scattering of photon and electrons. As mentioned previously in this chapter and noted by authors in various literatures, the accuracy of dose calculation algorithms is rated as principle-based algorithms such as Monte Carlo, and the linear Boltzmann transport as the most accurate, followed by model-based algorithms such as CCC, AAA, and PBC in that order for accuracy; and correction-based algorithms. Another important item to be considered is the beam modeling which will directly affect the accuracy of dose calculation where each TPS has its own features to model beams. Therefore, following the beam data measurements, commissioning of the modeled beams becomes a necessary step typically achieved through end-to-end testing. This is to verify dose distribution and accurate computation under different clinical conditions before any clinical use. Moreover, it is important to understand the response and limitations of each equipment used along with gamma index analysis due to different combinations

of QA devices and software packages, which may result in varying levels of agreement with the predicted gamma analysis for the same pass-rate criteria. Various reasons result in different correlations between GPR and complexity metrics, hence, these correlations are not generic and should be defined for each TPS.

### **Conflict of interest**

None to report.


### **Author details**

E. Ishmael Parsai and Elahheh Salari  
Department of Radiation Oncology, University of Toledo Medical Center, Toledo,  
Ohio, USA

\*Address all correspondence to: [e.parsai@utoledo.edu](mailto:e.parsai@utoledo.edu)

### **IntechOpen**

---

© 2022 The Author(s). Licensee IntechOpen. This chapter is distributed under the terms of the Creative Commons Attribution License (<http://creativecommons.org/licenses/by/3.0>), which permits unrestricted use, distribution, and reproduction in any medium, provided the original work is properly cited. 



## References

- [1] Khan F, Gerbi B. Treatment planning algorithms: Model-based photon dose calculations. *Treatment Planning in Radiation Oncology*. 2012;**1(3 ed)**:93-110
- [2] Liu HH, Mackie TR, McCullough EC. A dual source photon beam model used in convolution/superposition dose calculations for clinical megavoltage x-ray beams. *Medical Physics*. 1997;**24(12)**:1960-1974
- [3] Cashmore J. The characterization of unflattened photon beams from a 6 MV linear accelerator. *Physics in Medicine and Biology*. 2008;**53(7)**:1933-1946
- [4] Zhu XR, Kang Y, Gillin MT. Measurements of in-air output ratios for a linear accelerator with and without the flattening filter. *Medical Physics*. 2006;**33(10)**:3723-3733
- [5] Cho W, Kielar KN, Mok E, Xing L, Park JH, Jung WG, et al. Multisource modeling of flattening filter free (FFF) beam and the optimization of model parameters. *Medical Physics*. 2011;**38(4)**:1931-1942
- [6] Papanikolaou N, Battista JJ, Boyer A, Kappas C, Klein E, Mackie TR, et al. Tissue inhomogeneity corrections for megavoltage photon beams. In: Report of Task Group No 65 of the Radiation Therapy Committee of the American Association of Physicists in Medicine. Vernon Boulevard, Madison, USA: *Medical Physics*. 2004
- [7] Papanikolaou N, Stathakis S. Dose-calculation algorithms in the context of inhomogeneity corrections for high energy photon beams. *Medical Physics*. 2009;**36(10)**:4765-4775
- [8] Batho HF. Lung corrections in cobalt 60 beam therapy. *Journal of the Canadian Association of Radiologists*. 1964;**15**:79-83
- [9] Sontag MR, Cunningham JR. Corrections to absorbed dose calculations for tissue inhomogeneities. *Medical Physics*. 1977;**4(5)**:431-436
- [10] El-Khatib E, Battista JJ. Improved lung dose calculation using tissue-maximum ratios in the Batho correction. *Medical Physics*. 1984;**11(3)**:279-286
- [11] Thomas SJ. A modified power-law formula for inhomogeneity corrections in beams of high-energy x rays. *Medical Physics*. 1991;**18(4)**:719-723
- [12] Ahnesjo A, Aspradakis MM. Dose calculations for external photon beams in radiotherapy. *Physics in Medicine and Biology*. 1999;**44(11)**:R99-R155
- [13] Kappas K, Rosenwald JC. Theoretical and experimental analysis of scatter from inhomogeneous slabs in a  $^{60}\text{Co}$  beam: The differential tissue-air ratio method (DTAR). *Physics in Medicine and Biology*. 1986;**31(11)**:1211-1228
- [14] Mohan R, Chui C, Lidofsky L. Differential pencil beam dose computation model for photons. *Medical Physics*. 1986;**13(1)**:64-73
- [15] Elcim Y, Dirican B, Yavas O. Dosimetric comparison of pencil beam and Monte Carlo algorithms in conformal lung radiotherapy. *Journal of Applied Clinical Medical Physics*. 2018;**19(5)**:616-624
- [16] Kim DW, Park K, Kim H, Kim J. History of the photon beam dose calculation algorithm in radiation treatment planning system. *Progress in Medical Physics*. 2020;**3(31)**:54-62

- [17] Boyer AL, Mok EC. Calculation of photon dose distributions in an inhomogeneous medium using convolutions. *Medical Physics*. 1986; **13**(4):503-509
- [18] Zhu Y, Boyer AL. X-ray dose computations in heterogeneous media using 3-dimensional FFT convolution. *Physics in Medicine and Biology*. 1990; **35**:351-368
- [19] Wong E, Zhu Y, Van Dyk J. Theoretical developments on fast Fourier transform convolution dose calculations in inhomogeneous media. *Medical Physics*. 1996; **23**(9):1511-1521
- [20] Wong E, Van Dyk J, Zhu Y. Lateral electron transport in FFT photon dose calculations. *Medical Physics*. 1997; **24**(12):1992-2000
- [21] Ahnesjö A, Andreo P, Brahme A. Calculation and application of point spread functions for treatment planning with high energy photon beams. *Acta Oncologica*. 1987; **26**(1):49-56
- [22] Mack A, Weltz D, Scheib SG, Wowra B, Bottcher H, Seifert V. Development of a 3-D convolution/superposition algorithm for precise dose calculation in the skull. *Australasian Physical & Engineering Sciences in Medicine*. 2006; **29**(1):1-12
- [23] Ulmer W, Pyyry J, Kaissl W. A 3D photon superposition/convolution algorithm and its foundation on results of Monte Carlo calculations. *Physics in Medicine and Biology*. 2005; **50**(8):1767-1790
- [24] Tillikainen L, Helminen H, Torsti T, Siljamäki S, Alakuijala J, Pyyry J, et al. A 3D pencil-beam-based superposition algorithm for photon dose calculation in heterogeneous media. *Physics in Medicine and Biology*. 2008; **53**(14):3821-3839
- [25] Sievinen J, Ulmer W, Kaissl W. AAA Photon dose calculation model in eclipse™. Palo Alto: Varian Medical System; 2005
- [26] Knoos T, Wieslander E, Cozzi L, Brink C, Fogliata A, Albers D, et al. Comparison of dose calculation algorithms for treatment planning in external photon beam therapy for clinical situations. *Physics in Medicine and Biology*. 2006; **51**(22):5785-5807
- [27] Sterpin E, Tomsej M, De Smedt B, Reynaert N, Vynckier S. Monte Carlo evaluation of the AAA treatment planning algorithm in a heterogeneous multilayer phantom and IMRT clinical treatments for an Elekta SL25 linear accelerator. *Medical Physics*. 2007; **34**(5):1665-1677
- [28] Robinson D. Inhomogeneity correction and the analytic anisotropic algorithm. *Journal of Applied Clinical Medical Physics*. 2008; **9**(2):112-122
- [29] Ono K, Endo S, Tanaka K, Hoshi M, Hirokawa Y. Dosimetric verification of the anisotropic analytical algorithm in lung equivalent heterogeneities with and without bone equivalent heterogeneities. *Medical Physics*. 2010; **37**(8):4456-4463
- [30] Gete E, Teke T, Kwa W. Evaluation of the AAA treatment planning algorithm for SBRT lung treatment: Comparison with Monte Carlo and Homogeneous pencil beam dose calculations. *Journal of Medical Imaging and Radiation Sciences*. 2012; **43**(1):26-33
- [31] Panettieri V, Barsoum P, Westermark M, Brualla L, Lax I. AAA and PBC calculation accuracy in the surface build-up region in tangential beam treatments. Phantom and breast

case study with the Monte Carlo code PENELOPE. *Radiotherapy and Oncology*. 2009;**93**(1):94-101

[32] Bragg CM, Conway J. Dosimetric verification of the anisotropic analytical algorithm for radiotherapy treatment planning. *Radiotherapy and Oncology*. 2006;**81**(3):315-323

[33] Ahnesjo A. Collapsed cone convolution of radiant energy for photon dose calculation in heterogeneous media. *Medical Physics*. 1989;**16**(4):577-592

[34] De Martino F, Clemente S, Graeff C, Palma G, Cella L. Dose calculation algorithms for external radiation therapy: An overview for practitioners. *Applied Sciences*. 2021;**11**(15). DOI: 10.3390/app11156806

[35] Jeraj R, Keall P. The effect of statistical uncertainty on inverse treatment planning based on Monte Carlo dose calculation. *Physics in Medicine and Biology*. 2000;**45**(12): 3601-3613

[36] Vassiliev ON, Wareing TA, McGhee J, Failla G, Salehpour MR, Mourtada F. Validation of a new grid-based Boltzmann equation solver for dose calculation in radiotherapy with photon beams. *Physics in Medicine and Biology*. 2010;**55**(3): 581-598

[37] Han T, Followill D, Mikell J, Repchak R, Molineu A, Howell R, et al. Dosimetric impact of Acuros XB deterministic radiation transport algorithm for heterogeneous dose calculation in lung cancer. *Medical Physics*. 2013;**40**(5):051710

[38] Yan C, Combine AG, Bednarz G, Lalonde RJ, Hu B, Dickens K, et al. Clinical implementation and evaluation of the Acuros dose calculation algorithm.

*Journal of Applied Clinical Medical Physics*. 2017;**18**(5):195-209

[39] LoSasso T, Chui CS, Ling CC. Physical and dosimetric aspects of a multileaf collimation system used in the dynamic mode for implementing intensity modulated radiotherapy. *Medical Physics*. 1998;**25**(10): 1919-1927

[40] Cadman P, Bassalow R, Sidhu NP, Ibbott G, Nelson A. Dosimetric considerations for validation of a sequential IMRT process with a commercial treatment planning system. *Physics in Medicine and Biology*. 2002; **47**(16):3001-3010

[41] IAEA. TecDoc 1540: Specification and Acceptance Testing of Radiotherapy Treatment Planning Systems. Vienna: IAEA; 2007

[42] IAEA. TecDoc 1583: Commissioning of Radiotherapy Treatment Planning Systems: Testing for Typical External Beam Treatment Techniques. Vienna: IAEA; 2008

[43] Ezzell GA, Burmeister JW, Dogan N, LoSasso TJ, Mechalakos JG, Mihailidis D, et al. IMRT commissioning: Multiple institution planning and dosimetry comparisons, a report from AAPM task group 119. *Medical Physics*. 2009;**36**(11): 5359-5373

[44] Zhang Y, Le AH, Tian Z, Iqbal Z, Chiu T, Gu X, et al. Modeling Elekta VersaHD using the Varian eclipse treatment planning system for photon beams: A single-institution experience. *Journal of Applied Clinical Medical Physics*. 2019;**20**(10):33-42

[45] Middlebrook ND, Sutherland B, Kairn T. Optimization of the dosimetric leaf gap for use in planning VMAT

treatments of spine SABR cases. *Journal of Applied Clinical Medical Physics*. 2017;**18**(4):133-139

[46] Shende R, Patel G. Validation of Dosimetric leaf gap (DLG) prior to its implementation in treatment planning system (TPS): TrueBeam millennium 120 leaf MLC. *Reports of Practical Oncology and Radiotherapy*. 2017;**22**(6):485-494

[47] Kim J, Han JS, Hsia AT, Li S, Xu Z, Ryu S. Relationship between dosimetric leaf gap and dose calculation errors for high definition multi-leaf collimators in radiotherapy. *Physics and Imaging in Radiation Oncology*. 2018;**5**: 31-36

[48] Mzenda B, Mugabe KV, Sims R, Godwin G, Loria D. Modeling and dosimetric performance evaluation of the RayStation treatment planning system. *Journal of Applied Clinical Medical Physics*. 2014;**15**(5):4787

[49] Chen S, Yi BY, Yang X, Xu H, Prado KL, D'Souza WD. Optimizing the MLC model parameters for IMRT in the RayStation treatment planning system. *Journal of Applied Clinical Medical Physics*. 2015;**16**(5):322-332

[50] Miften M, Olch A, Mihailidis D, Moran J, Pawlicki T, Molineu A, et al. Tolerance limits and methodologies for IMRT measurement-based verification QA: Recommendations of AAPM task group No. 218. *Medical Physics*. 2018; **45**(4):e53-e83

[51] Low DA, Harms WB, Mutic S, Purdy JA. A technique for the quantitative evaluation of dose distributions. *Medical Physics*. 1998; **25**(5):656-661

[52] Park JM, Kim JI, Park SY, Oh DH, Kim ST. Reliability of the gamma index

analysis as a verification method of volumetric modulated arc therapy plans. *Radiation Oncology*. 2018;**13**(1):175

[53] Bailey DW, Nelms BE, Attwood K, Kumaraswamy L, Podgorsak MB. Statistical variability and confidence intervals for planar dose QA pass rates. *Medical Physics*. 2011;**38**(11):6053-6064

[54] Depuydt T, Van Esch A, Huyskens DP. A quantitative evaluation of IMRT dose distributions: Refinement and clinical assessment of the gamma evaluation. *Radiotherapy and Oncology*. 2002;**62**(3):309-319

[55] Wendling M, Zijp LJ, McDermott LN, Smit EJ, Sonke JJ, Mijnheer BJ, et al. A fast algorithm for gamma evaluation in 3D. *Medical Physics*. 2007;**34**(5):1647-1654

[56] Ju T, Simpson T, Deasy JO, Low DA. Geometric interpretation of the gamma dose distribution comparison technique: Interpolation-free calculation. *Medical Physics*. 2008;**35**(3):879-887

[57] Low DA, Dempsey JF. Evaluation of the gamma dose distribution comparison method. *Medical Physics*. 2003;**30**(9): 2455-2464

[58] Schreiner LJ, Salomons G, Holmes O. Analysis and evaluation of planned and delivered dose distributions: Practical concerns with  $\gamma$ - and  $\chi$ - evaluations. *Journal of Physics Conference Series (Online)*. 2013;**444**(1):9

[59] Bruschi A, Esposito M, Pini S, Ghirelli A, Zatelli G, Russo S. How the detector resolution affects the clinical significance of SBRT pre-treatment quality assurance results. *Physica Medica*. 2018;**49**:129-134

[60] Stathakis S, Myers P, Esquivel C, Mavroidis P, Papanikolaou N.

Characterization of a novel 2D array dosimeter for patient-specific quality assurance with volumetric arc therapy. *Medical Physics*. 2013;**40**(7):071731

[61] Woon W, Ravindran PB, Ekayanake P, SV, Lim YY, Khalid J. A study on the effect of detector resolution on gamma index passing rate for VMAT and IMRT QA. *Journal of Applied Clinical Medical Physics*. 2018;**19**(2): 230-248

[62] Steers JM, Fraass BA. IMRT QA and gamma comparisons: The impact of detector geometry, spatial sampling, and delivery technique on gamma comparison sensitivity. *Medical Physics*. 2021;**48**(9):5367-5381

[63] Salari E, Parsai EI, Shvydka D, Sperling N. Evaluation of parameters affecting gamma passing rate in patient-specific QA's for multiple brain lesions IMRS treatments using Ray-Station treatment planning system. *Journal of Applied Clinical Medical Physics*. 2021;**23**(1):e13467. DOI: 10.1002/acm2.13467

[64] Hussein M, Rowshanfarzad P, Ebert MA, Nisbet A, Clark CH. A comparison of the gamma index analysis in various commercial IMRT/VMAT QA systems. *Radiotherapy and Oncology*. 2013;**109**(3):370-376

[65] Masi L, Doro R, Favuzza V, Cipressi S, Livi L. Impact of plan parameters on the dosimetric accuracy of volumetric modulated arc therapy. *Medical Physics*. 2013;**40**(7): 071718

[66] Nicolini G, Clivio A, Cozzi L, Fogliata A, Vanetti E. On the impact of dose rate variation upon RapidArc implementation of volumetric modulated arc therapy. *Medical Physics*. 2011;**38**(1):264-271

[67] Wu S, Chen J, Li Z, Qiu Q, Wang X, Li C, et al. Analysis of dose verification results for 924 intensity-modulated radiation therapy plans. *Precision Radiation Oncology*. 2018;**2**:125-130

[68] McNiven AL, Sharpe MB, Purdie TG. A new metric for assessing IMRT modulation complexity and plan deliverability. *Medical Physics*. 2010; **37**(2):505-515

[69] Rajasekaran D, Jeevanandam P, Sukumar P, Ranganathan A, Johnjothi S, Nagarajan V. A study on the correlation between plan complexity and gamma index analysis in patient specific quality assurance of volumetric modulated arc therapy. *Reports of Practical Oncology and Radiotherapy*. 2015;**20**(1):57-65

[70] Glenn MC, Hernandez V, Saez J, Followill DS, Howell RM, Pollard-Larkin JM, et al. Treatment plan complexity does not predict IROC Houston anthropomorphic head and neck phantom performance. *Physics in Medicine and Biology*. 2018;**63**(20): 205015

[71] Hernandez V, Saez J, Pasler M, Jurado-Bruggeman D, Jornet N. Comparison of complexity metrics for multi-institutional evaluations of treatment plans in radiotherapy. *Physics and Imaging in Radiation Oncology*. 2018;**5**:37-43

[72] Younge KC, Matuszak MM, Moran JM, McShan DL, Fraass BA, Roberts DA. Penalization of aperture complexity in inversely planned volumetric modulated arc therapy. *Medical Physics*. 2012;**39**(11):7160-7170

[73] Du W, Cho SH, Zhang X, Hoffman KE, Kudchadker RJ. Quantification of beam complexity in intensity-modulated radiation therapy

treatment plans. *Medical Physics*. 2014;  
**41**(2):021716

window and VMAT techniques. *Medical Physics*. 2015;**42**(4):1911-1916

[74] Park JM, Park SY, Kim H, Kim JH, Carlson J, Ye SJ. Modulation indices for volumetric modulated arc therapy. *Physics in Medicine and Biology*. 2014;  
**59**(23):7315-7340

[81] Van Esch A, Huyskens DP, Behrens CF, Samsøe E, Sjolín M, Bjelkengren U, et al. Implementing RapidArc into clinical routine: A comprehensive program from machine QA to TPS validation and patient QA. *Medical Physics*. 2011;**38**(9):5146-5166

[75] Webb S. Use of a quantitative index of beam modulation to characterize dose conformality: Illustration by a comparison of full beamlet IMRT, few-segment IMRT (fsIMRT) and conformal unmodulated radiotherapy. *Physics in Medicine and Biology*. 2003;**48**(14): 2051-2062

[76] Crowe SB, Kairn T, Kenny J, Knight RT, Hill B, Langton CM, et al. Treatment plan complexity metrics for predicting IMRT pre-treatment quality assurance results. *Australasian Physical & Engineering Sciences in Medicine*. 2014;**37**(3):475-482

[77] Heilemann G, Poppe B, Laub W. On the sensitivity of common gamma-index evaluation methods to MLC misalignments in Rapidarc quality assurance. *Medical Physics*. 2013;**40**(3): 031702

[78] Nauta M, Villarreal-Barajas JE, Tambasco M. Fractal analysis for assessing the level of modulation of IMRT fields. *Medical Physics*. 2011;  
**38**(10):5385-5393

[79] Wu S, Chen J, Li Z, Qiu Q, Wang X, Li C, et al. Analysis of dose verification results for 924 intensity-modulated radiation therapy plans. *Precision Radiation Oncology*. 2018;**2**(4):125-130

[80] Hernandez V, Abella R, Calvo JF, Jurado-Bruggemann D, Sancho I, Carrasco P. Determination of the optimal tolerance for MLC positioning in sliding